Embedded Stellar Clusters in the W3/W4/W5 Molecular Cloud Complex

John M. Carpenter
email: jmc@astro.caltech.edu

California Institute of Technology, Department of Astronomy, MS 105-24, Pasadena, CA 91125

Mark H. Heyer
email: heyer@fermat.astro.umass.edu

and

Ronald L. Snell
email: snell@fcrao1.astro.umass.edu

University of Massachusetts, Department of Astronomy, Amherst, MA 01003

ABSTRACT

We analyze the embedded stellar content in the vicinity of the W3/W4/W5 H II regions using the FCRAO Outer Galaxy ^{12}CO(1–0) Survey, the IRAS Point Source Catalog, published radio continuum surveys, and new near-infrared and molecular line observations. Thirty-four IRAS Point Sources are identified that have far-infrared colors characteristic of embedded star forming regions, and we have obtained K' mosaics and ^{13}CO(1–0) maps for 32 of them. Ten of the IRAS sources are associated with an OB star and 19 with a stellar cluster, although three OB stars are not identified with a cluster. Half of the embedded stellar population identified in the K' images is found in just the 5 richest clusters, and 61% is contained in IRAS sources associated with an embedded OB star. Thus rich clusters around OB stars contribute substantially to the stellar population currently forming in the W3/W4/W5 region. Approximately 39% of the cluster population is embedded in small clouds with an average mass of $\approx 130\,M_\odot$ that are located as far as 100 pc from the W3/W4/W5 cloud complex. We speculate that these small clouds are fragments of a cloud complex dispersed by previous episodes of massive star formation. Finally, we find that 4 of the 5 known embedded massive star forming sites in the W3 molecular cloud are found along the interface with the W4 H II region despite the fact that most of the molecular mass is contained in the interior regions of the cloud. These observations are consistent with the classical notion that the W4 H II region has triggered massive star formation along the eastern edge of the W3 molecular cloud.

Subject headings: infrared: stars — ISM: individual (W3,W4,W5) — stars: formation stars — pre-main-sequence

1. Introduction

The equilibrium of molecular clouds is frequently perturbed by passages through spiral arms, cloud-cloud collisions, shocks from OB stellar winds and ionization fronts, molecular outflows, and other energetic forces. Depending on the local conditions, these events can either compress or disperse the molecular cloud, and consequently, induce or halt any future star formation (Elmegreen 1992). These interactions occur more frequently among clouds located in the disk of the Milky Way, and therefore potentially, the average star formation characteristics of clouds in the disk can differ from those that are far removed from the Galactic Plane. Since most of the molecular material is confined to the disk of the Galaxy (Clemens, Sanders, & Scoville 1988; Dame et al. 1987), studying the stellar content of Galactic Plane molecular clouds is necessary to establish the conditions under which most star form.

The biggest challenge in studying molecular clouds in the disk of the Galaxy is that they are generally rather distant from the sun at several kiloparsecs and are often blended together in projection, especially in the inner Galaxy (see, e.g., Lee, Snell, & Dickman 1990). Thus detecting and uniquely associating star formation sites within individual molecular clouds can often be problematic. To minimize these difficulties, the Five College Radio Astronomy Observatory (FCRAO) has recently completed a ^{12}CO survey of the Outer Galaxy (Heyer et al. 1998). This survey encompasses $330\,\mathrm{deg}^2$ of the second Galactic quadrant at subarcminute resolution and sampling, and represents the most detailed examination to date of the molecular interstellar medium. Most lines of sight in the survey contain a single molecular cloud, and moreover, this region of the Galaxy includes the closest approach of the Perseus Spiral Arm to the sun at a distance of $\approx 2\,\mathrm{kpc}$ (Georgelin & Georgelin 1976). In these respects, this is one of the best regions in the Milky Way to investigate the stellar properties of Galactic Plane molecular clouds.

In this paper, we investigate the stellar characteristics of molecular clouds within the Perseus Spiral Arm, and more specifically, clouds in the vicinity of the W3/W4/W5 H II regions, using the FCRAO Outer Galaxy ^{12}CO Survey, the IRAS Point Source Catalog, published radio continuum observations, and new near-infrared and molecular line data. The W3/W4/W5 chain of H II regions is ionized by members of the Cas OB6 association and extends over 150 pc along the Perseus Arm. The winds and ionizing flux from the massive stars have clearly impacted the interstellar medium by creating a galactic chimney out of the atomic hydrogen gas (Normandeau, Taylor, & Dewdney 1996), shaping molecular clouds into cometary globules with parsec sized tails (Heyer et al. 1996), and possibly inducing a second generation of OB star formation (Lada et al. 1978; Thronson, Campbell, & Hoffman 1980). Despite the vigorous star formation activity in the past, a substantial mass of molecular gas remains (Heyer & Terebey 1998; Digel et al. 1996; Lada et al. 1978). The W3 molecular cloud alone has $\approx 10^5\,\mathrm{M}_\odot$ of molecular material spread over a $\approx 60\,\mathrm{pc}$ region (Deane et al. 2000; Lada et al. 1978) and is one of the most massive molecular clouds in the outer Galaxy (Heyer et al. 1998). The luminous star forming sites W3 Main, W3(OH), W3 North, and AFGL 333 (Thronson, Campbell, & Hoffman 1980), a ridge of dense molecular gas (Tieftrunk et al. 1998), and the presence of embedded clusters throughout the W3/W4/W5 cloud complex

(Tieftrunk et al. 1998; Deharveng et al. 1997; Megeath et al. 1996; Hodapp 1994; Carpenter et al. 1993) all attest to the continued star formation activity in this region. In addition to the massive W3 Giant Molecular Cloud (GMC), a number of small clouds with similar ^{12}CO(1–0) velocities as the W3/W4/W5 region are found scattered throughout the area (Heyer et al. 1998).

To investigate the most recent generation of star formation throughout the W3/W4/W5 region, we have selected a sample of likely embedded star forming sites using the IRAS point source catalog. In conjunction with new ^{13}CO(1–0) and K' band near-infrared observations, we investigate the spatial distribution of star forming regions, their associated molecular cloud properties, and the incidence of stellar clusters, and use these data to establish where most of the stars are now forming in the W3/W4/W5 region. These results are presented as follows. Section 2 discusses the criteria used to identify star forming regions from the IRAS Point Source Catalog and describe the observations and data reduction procedures for the new molecular line and near-infrared surveys. In Section 3, we characterize the stellar content associated with the IRAS sources based upon the far-infrared luminosity, published radio continuum observations, and the incidence of any stellar clusters detected in the K' band mosaics. The implication of these results on star formation in the W3/W4/W5 region is discussed in Section 4, and our conclusions are summarized in Section 5.

2. Observations

The region analyzed for this study encompasses the area between galactic longitudes $\ell = 130°$ to 139° and latitudes $b = -2.2°$ to $+4.5°$. Figures 1 and 2 show this region of the Galaxy as observed in ^{12}CO(1–0) from the FCRAO Outer Galaxy Survey (Heyer et al. 1998) and in $\lambda\,21\,\mathrm{cm}$ radio continuum emission from the DRAO Galactic Plane Survey (Normandeau, Taylor, & Dewdney 1997). The W3, W4, and W5 H II regions and the associated molecular clouds are evident in these figures. A list of candidate embedded star forming regions within these clouds were selected using the IRAS point source catalog, and follow-up observations of these sources were conducted to ascertain their stellar content. The selection criteria for the IRAS point sources and the ancillary observations are described below.

2.1. IRAS Point Source Selection

Guided by the far-infrared colors of known embedded star forming regions (Carpenter, Snell, & Schloerb 1991; Kenyon et al. 1990; Beichman et al. 1986) and the properties of the IRAS sources observed by Wouterloot et al. (1990), the following five criteria were used to identify embedded star forming regions in the IRAS Point Source Catalog, Version 2.1. (1) The source has a high or moderate quality flux measurement at both $25\,\mu$m and $60\,\mu$m. (2) The flux density at $25\,\mu$m is $\geq 0.4\,$Jy. (3) The flux density at $60\,\mu$m is $\geq 1.0\,$Jy. (4) The ratio of the $60\,\mu$m to the $25\,\mu$m flux density is > 1.0. (5) The ratio of the $100\,\mu$m to the $60\,\mu$m flux density is ≤ 4.0. The two flux

density ratio criteria were designed to isolate sources with rising spectral energy distributions, but to eliminate the reddest objects that are often indicative of infrared cirrus. Any upper limits to the 100 μm flux density were used as appropriate in evaluating the ratios.

Of the sources meeting the above criteria, 34 were identified with a molecular cloud that has a ^{12}CO velocity between -57 km s^{-1} $\leq v_{\rm lsr} \leq$ -32 km s^{-1} and are likely in the Perseus spiral arm (Heyer et al. 1998). These 34 sources are listed in Table 1, along with the galactic and equatorial coordinates, the velocity of the ^{12}CO(1–0) emission coincident with the IRAS source, and any source identifications. All but two of these sources, as noted in Table 1, were imaged at K' band and mapped in ^{13}CO as described below. The spatial distribution of the IRAS point sources is shown by the open circles in Figure 1, where the circle diameter is proportional to the far-infrared luminosity (see Section 3.2). The source list does not include W3 Main, which is confused at 60 μm in the IRAS survey and did not meet the selection criteria. Near-infrared observations of this source have been presented by Megeath et al. (1996; see also Tieftrunk et al. 1998 and Hodapp 1994). Also, two of the IRAS sources have previously been associated with galaxies (Weinberger 1980). However, the strong ^{12}CO emission and the apparent stellar cluster (see Section 4.1) associated with these two sources suggests that the far-infrared emission originates from embedded stars and not an extragalactic object.

2.2. K' Band Imaging

Near-infrared mosaics in a K' band filter (Wainscoat & Cowie 1992) were obtained for 32 of the 34 IRAS sources in Table 1. Time constraints prevented us from observing IRAS 02081+6225 and 02204+6128. The images were obtained over a two night period in 1996 October using QUIRC at the University of Hawaii 2.24 m telescope on Mauna Kea through thin cirrus with seeing conditions of $\approx$0.5-0.6″. QUIRC contains a 1024 $\times$ 1024 HgCdTe array and was used at the $f/10$ focus to provide a plate scale of 0.186″ pixel^{-1} and an instantaneous field of view of 3.2′ $\times$ 3.2′. For each IRAS source, a 5′ $\times$ 5′ mosaic aligned in the equatorial coordinate system was obtained that consists of 12 dithered frames with an exposure time of 30 seconds per frame. Sky frames were constructed by median filtering images free of extended nebulosity. The sky-subtracted frames were then corrected by a flat field image derived from a series of exposures of the dome interior with and without illumination from incandescent lights. In constructing the mosaics, three frames were coadded per pixel position in the mosaic in order to maintain a constant noise level across the final image. Coadded pixels near the edge of the mosaic that have only one or two observations were discarded. Astrometry for 23 of the 32 mosaics (see Table 1) were established using images from the 2 Micron All Sky Survey (2MASS). 2MASS images for the 9 remaining mosaics were not available at the time of this study, and we assumed that the center of these mosaics corresponds to the IRAS point source position. Based on the results from registering the 23 mosaics with available 2MASS images, we expect that the astrometry for these 9 mosaics to be accurate to be $\leq$ 30″.

Stars were identified in the mosaics using DAOFIND in IRAF. The noise for each mosaic was measured empirically, and a 5σ detection threshold was used to create an initial source list. All mosaics were then visually inspected to remove a few saturated stars and any obvious non-stellar objects (e.g. ghosts, nebulosity knots), and to add any stars that were not identified by DAOFIND. Photometry was performed using the point-spread fitting task DAOPHOT in IRAF. The point spread function (PSF) was determined for each mosaic using several bright, isolated stars in the image. After fitting the PSF to each star in the point source list and subtracting the fit from the mosaic, the resulting image was examined for any additional point sources that were initially missed due to source confusion. These stars were added to the detection list and were also measured using DAOPHOT. Finally, objects identified by DAOPHOT as being unusually extended based upon the "sharp" statistic (e.g. galaxies, nebulosity) were removed form the point source list. The number of extended objects removed by this criteria amounted to less than 10% of the total number of sources identified. The photometry was calibrated by observing standard stars in the UKIRT faint standards list (Casali & Hawarden 1992) and assuming a K' band extinction coefficient of 0.08 mag/airmass. The RMS scatter over the two nights in the photometric zero points derived from the standard observations is 3%.

The differential completeness limit of the survey was established by adding artificial stars of known magnitude to one of the mosaics and determining the fraction of the stars that could be recovered at the 5σ detection threshold. When adding artificial stars, care was taken not to add objects near a known star or within nebulous regions. The completeness limit in these more confused regions will obviously occur at a brighter magnitude. Approximately 90% of the stars with a K' magnitude of $17.5^{\rm m}$ were recoverable in this automated procedure. The star counts analyzed in the paper are therefore for objects with K' magnitudes between $11.5^{\rm m}$ (the saturation limit) and $17.5^{\rm m}$.

2.3. ^{13}CO Mapping

A region of size $(\Delta\ell \times \Delta b) = (6.2' \times 4.8')$ toward the 32 IRAS point sources was mapped in ^{13}CO(1–0) (110.201370 GHz) using the SEQUOIA receiver array on the 14 m telescope operated by the Five College Radio Astronomy Observatory (FCRAO) in the spring of 1998. At the time of the observations, SEQUOIA had 12 pixel elements. The full-width-at-half-maximum (FWHM) beam size of the FCRAO telescope at the observed frequency is $47''$, and the maps were sampled every $22''$, or approximately the Nyquist sampling interval. The backends for each pixel in the SEQUOIA array consisted of an autocorrelator spectrometer configured to achieve a velocity resolution of $0.064\,{\rm km\,s^{-1}}$ over a $54\,{\rm km\,s^{-1}}$ velocity interval. The data were obtained in frequency switching mode with an offset of 4 MHz between the nominal and reference frequency. The ^{13}CO data presented here have been corrected by the main beam efficiency, previously measured to be $\eta_{\rm B} = 0.45$. The RMS noise is typically $\Delta T_{\rm MB} = 0.7$-1.1 K per channel.

3. Results

3.1. Images

Molecular line and K' band images of the 32 IRAS point sources observed for this study are shown in Figure 3. Four images are shown for each IRAS source: (1) a ^{12}CO(1–0) integrated intensity map from the FCRAO Outer Galaxy Survey over a $30' \times 30'$ area centered on the IRAS point source position (far left panels), (2) the ^{13}CO integrated intensity map over a $6.2' \times 4.8'$ region, (3) the K' band mosaic, and (4) the K' stellar surface density map. The ^{12}CO images are shown over a larger extent than the ^{13}CO maps and K' band mosaics in order to place the IRAS source in context of the large scale molecular cloud in the region. Figure 3 indicates that most of the ^{13}CO maps peak near the IRAS point source positions and suggests that the IRAS sources are indeed related with the molecular gas. In the remainder of this section, we characterize the stellar population associated with these IRAS sources as inferred from the far-infrared luminosity, the presence of an embedded massive star as indicated by radio continuum emission, and the identification of stellar clusters from K' band star counts.

3.2. Far-Infrared Luminosities

The stellar content associated with the IRAS sources can be constrained to first order by assuming that dust absorbs a substantial fraction of the stellar bolometric luminosity and re-emits the radiation in the far-infrared. Since many of the IRAS sources are associated with a cluster of stars (see Section 3.4), the far-infrared emission actually sets a limit on the most massive star that may be forming in these regions. The luminosity emitted in the 12 μm, 25 μm, 60 μm bands (L_{FIR}) was computed by summing the observed flux densities in the individual IRAS band passes using the formula

$$\begin{aligned} L_{FIR} &= 4\pi D^2 \sum_i (S_{\nu i}\, \Delta\nu_i) \\ &= 0.30 \left(\frac{D}{kpc}\right)^2 \sum_i \left(\frac{S_{\nu i}}{Jy}\right) \left(\frac{\Delta\nu_i}{10^{12}\ Hz}\right) L_\odot, \end{aligned} \quad (1)$$

where D is the distance to the source in kiloparsecs (assumed to be 2.35 kpc; Massey, Johnson, & DeGioia-Eastwood 1995), $\Delta\nu$ the IRAS band width, and S_ν the observed flux density. The sum does not extend over the 100 μm band since many sources are confused at 100 μm and this band could not be applied consistently for the entire sample. Thus the computed far-infrared luminosities (see column 2 in Table 2) will underestimate the actual bolometric and far-infrared luminosities. For IRAS sources in the W3/W4/W5 region that do have high quality 100 μm detections, we found that the 12 μm-60 μm luminosity underestimates the total IRAS far-infrared luminosity by $\approx$30% on average.

A histogram of the derived far-infrared luminosities for the 34 IRAS sources is shown in Figure 4. The observed luminosities range between $9\,L_\odot$ and $46{,}000\,L_\odot$ with the peak of the distribution at $\approx 100\,L_\odot$. The brightest sources have luminosities similar to that of early B type zero age main sequence (ZAMS) stars (Panagia 1973) assuming that most of the far-infrared luminosity originates from a single object. The lowest luminosities in the histogram are a result of the selection criteria. The flux density criteria alone used to select the IRAS sources implies a detection limit of $8\,L_\odot$. Further, since the $60\,\mu$m flux density is on average 11 times larger than the $25\,\mu$m flux density for sources in our sample, the detection limit set by the spectral energy distribution and flux density limits is $23\,L_\odot$. The decline in the number of sources with luminosities fainter than $\approx 100\,L_\odot$ then is likely a result of incompleteness in the IRAS point source catalog. This $100\,L_\odot$ limit corresponds to a 1 Myr, $3\,M_\odot$ pre-main-sequence object (Palla & Stahler 1993), or a late B ZAMS star.

3.3. Radio Continuum Emission

The stellar content associated with the IRAS sources can be further constrained by using radio continuum observations to estimate the spectral type of the most massive star. The list of radio continuum sources in the W3/W4/W5 region were taken primarily from the $\lambda\,20$ cm NRAO/VLA Sky Survey (NVSS; Condon et al. 1998), but also published targeted observations (Kurtz, Churchwell, & Wood 1994; McCutcheon et al. 1991; Carpenter, Snell, & Schloerb 1991). Sources in the NVSS catalog were deemed associated with an IRAS source if the radio and far-infrared coordinates agreed to within $30''$. While no spectral information is available from the NVSS catalog to confirm that these objects are actually compact H II regions, the random probability of a false association between an extragalactic radio continuum source and the IRAS point source is only ≈ 0.01 for the adopted $30''$ matching radius (Condon et al. 1998). The observed radio continuum flux was used to estimate the number of ionizing photons (see, e.g., Carpenter, Snell, & Schloerb 1991) and consequently the spectral type of the ionizing star (Panagia 1973). The inferred spectral types and references for the radio continuum observations are provided in columns 3 and 4 of Table 2. Ten of the 32 IRAS point sources have radio continuum detections, and the inferred spectral types range from B2 ZAMS to O7 ZAMS. If the stellar parameters from Vacca, Garmany, & Shull (1996) are used instead of Panagia (1973) to infer the spectral type, all but one of the detected sources will have a spectral type later than B0.5 ZAMS.

Two of the IRAS sources (IRAS 01546+6319 and 02511+6023) associated with a B type star as based on their radio continuum flux have a $12\,\mu$m-$60\,\mu$m luminosity that is 2 orders of magnitude less than that expected for such a massive star (Panagia 1973). Either the association between these radio continuum and IRAS sources is incorrect and the radio continuum source is an extragalactic object, or a substantial fraction of the bolometric luminosity is radiated at shorter wavelengths. The latter situation may occur if a star forming region is relatively evolved and the circumstellar dust no longer completely absorbs and re-emit the stellar radiation, although no obvious bright star

is present in the K' mosaics or on the Palomar Observatory Sky Survey prints to indicate that this may be the case. Nonetheless, we assume in the remainder of this paper these two IRAS sources are indeed massive star forming regions. Our general conclusions will not change if this assumption is incorrect.

3.4. Identification of Stellar Clusters

As another means to characterize the stellar content associated with the IRAS Point Sources, we searched for stellar clusters in the K' images using the procedure adopted by Carpenter, Snell, & Schloerb (1995; see also Carpenter et al. 1997). Briefly, histograms of the stellar field star density were generated for each mosaic using $20'' \times 20''$ counting bins sampled every $10''$. The observed frequency distribution of counts at low stellar surface densities in these histograms usually resembles a Poisson distribution, which is identified with field stars and embedded stars randomly distributed across the K' band mosaic. By fitting a Poisson distribution to these lower surface density bins, the mean stellar surface density of randomly distributed stars can be determined. Stellar surface density bins that significantly exceed this mean surface density are identified as possible clusters. Contour maps of the stellar surface density are shown in Figure 3 for each of the mosaics. The lowest contour in each map begin at 2σ for a Poisson distribution above the mean stellar surface density with 3σ contour intervals.

A cluster was identified in Figure 3 if the total number of stars within the 2σ contour represents a 5σ enhancement with respect to the expected stellar background level. Further, we require that the identified cluster be near the center of the mosaic and the IRAS point source position. In a few instances, apparent clusters were identified near the edge of the mosaic. In nearly all of these cases, the extinction through the cloud was large enough and variable that a Poisson distribution is a poor representation of the star counts, and these clusters most likely represent regions within the image where the extinction becomes low. Any such "cluster" is almost certainly a projection of unrelated field stars and was excluded from the final cluster list.

Table 2 summarizes the properties of the identified clusters, including the effective cluster radius ($R_{\rm eff}$), the number of stars observed within the 2σ boundary (N_s), and the number of stars inferred for the cluster after subtracting off the expected field star population ($N_{\rm cluster}$). The effective radius is defined as $\sqrt{A/\pi}$, where A is the area within the 2σ contour. Of the 32 IRAS sources, 19 have identifiable clusters, with the number of cluster members ranging from 20 to 240 stars. Our results agree with previous studies in that clusters are identified around IRAS 02232+6138 (Tieftrunk et al. 1998), IRAS 02575+6017 (Deharveng et al. 1997; Hodapp 1994; Carpenter et al. 1993), and IRAS 02593+6016 (Carpenter et al. 1993). However, Tieftrunk et al. (1998) visually noted a second cluster near IRAS 02232+6138 that is within the field of view of our mosaic. This grouping of stars does not meet the surface density criteria adopted here to be identified as a cluster.

The cluster membership listed in Table 2 are lower limits to the actual stellar population in these regions, mainly due to the finite sensitivity of the observations. To compare these clusters with other star forming regions, we computed the fraction of stars in nearby embedded clusters that would be detectable at the distance of W3 considering both differences in sensitivity and resolution. In the UKIRT survey of the MonR2 cluster by Carpenter et al. (1997), 246 of 378 stars (65%) would be detectable with our QUIRC observations at the distance of W3/W4/W5. Similarly, we could detect ≈ 410 (53%) of the ≈ 780 stars in the inner $5' \times 5'$ of the Orion Nebula Cluster (Hillenbrand & Carpenter 2000), and $\approx 75\%$ of the 94 stars brighter than $m_k = 14.5^{\rm m}$ in the NGC 1333 cluster (Lada, Alves, & Lada 1996). Assuming that the extinction toward the W3/W4/W5 clusters is not substantially different than toward these comparison regions, the richer W3/W4/W5 clusters (≈ 200 stars) are comparable to MonR2, but not as rich as the Orion Nebula Cluster. Several of the W3/W4/W5 clusters though have significantly fewer stars than these comparison regions.

3.5. Molecular Cloud Properties

The properties of the molecular clouds associated with the IRAS sources as derived from ^{13}CO(1–0) emission are summarized in Table 3. The cloud sizes are defined as the circular radius needed to produce the area within the FWHM integrated intensity contour. The cloud masses were computed from the integrated ^{13}CO(1–0) intensity by assuming that the emission is optically thin and that the $^{13}CO/H_2$ abundance is 1.5×10^{-6} (Bachiller & Cernicharo 1986). Statistical equilibrium calculations indicate that for H_2 volume densities between $300\,{\rm cm}^{-3}$ and $10^4\,{\rm cm}^{-3}$ and kinetic temperatures between 10 K and 20 K, the fraction of the ^{13}CO molecules in the J=1 rotational state varies between 0.41 to 0.54, and 0.48 was adopted as a typical value. A factor of 1.36 was included in the calculations to include the mass contribution from helium and other elements. The ^{13}CO integrated intensity used to calculate the masses includes the region within the FWHM intensity contour, but was also extrapolated to include emission outside this contour level by assuming a gaussian intensity distribution. Lower limits to the cloud sizes and masses are reported for sources in which the ^{13}CO maps did not completely encompass the half power contour level. The derived cloud masses range from $27\,{\rm M}_\odot$ to $> 3200\,{\rm M}_\odot$ (see Table 3). Many of these clouds, and in particular the more massive objects, are parts of the extended W3 and W5 GMCs. Several of the clouds are small and distant from any GMC (see Figure 1) and are nearly completely mapped with these ^{13}CO observations.

4. Discussion

4.1. Stellar Clusters in W3/W4/W5

From the results presented in Section 3 we can begin to assess the properties of the regions that are forming most of the cluster stellar population. The 19 identified clusters contain a total of 1595

stars within the $2\,\sigma$ boundary after subtracting off the expected field star contamination. (If the $1\,\sigma$ boundary is used to define the clusters, the total membership increases by 33%.) Figure 5 shows the normalized cumulative distribution of the total number of stars in all 19 clusters as a function of the number of stars in an individual cluster. As Figure 5 shows, 52% of the cluster members are found in just the 5 richest clusters. Even if we assume that the 13 IRAS sources without identified clusters have 20 stars each (the smallest population cluster identified in this survey), the 5 richest clusters would still contain 45% of the total cluster membership. These results do not change significantly if we include the W3 Main cluster, which has ≈ 87 stars to a comparable sensitivity limit as our survey (Megeath et al. 1996), or the other clusters identified along the W3 ridge (Tieftrunk et al. 1998).

We can also investigate the fraction of the cluster population associated with embedded OB stars. The 5 rich clusters described above that contain the majority of the cluster population are each associated with a massive star, and in total, clusters around OB stars contain 61% of the cluster population. Not all of the embedded OB stars though are associated with clusters. IRAS 02230+6202, 02511+6023, and 02531+6032 do not show a significant enhancement in the stellar surface density despite having a radio continuum detection. Based on the field star initial mass function, one would expect an OB type star to form along with a few hundred lower mass objects (Miller & Scalo 1979). It would be remarkable then if these regions are truly forming a single massive star, and would imply that the stellar mass function in these regions is strongly skewed toward high mass objects. With high spatial resolution data at only one wavelength, however, we cannot yet rule out the possibility that the lack of a cluster in these regions is merely due to a large amount of extinction, and additionally in the case IRAS 02230+6202, a bright nebular background (see Fig. 3), that prevents us from detecting the underlying cluster. Deeper observations in the near- and mid-infrared should be able to establish more definitively if these OB stars are truly forming in isolation.

In principle the above results could change if a large number of low luminosity IRAS sources exist that did not meet our selection criteria but contribute substantially to the cluster population. Based on the peak of the histogram in Figure 4, we assume that the luminosity completeness limit for the IRAS point sources is $\approx 200\,L_\odot$, and a power law function was fitted to the histogram bins more luminous than this limit. Extrapolation of this power fit suggests that there could be ≈ 40 additional sources between $10\,L_\odot$ and $200\,L_\odot$ that are not already in our sample. Even if we assume these sources have 20 stars each (the smallest cluster size detected here), the IRAS sources associated with OB will still contain more than a third of the total cluster population. These suggest indicate that the formation of dense stellar clusters surrounding OB stars represent a significant component of the cluster population in the W3/W4/W5 region.

Our results for the W3/W4/W5 region can be compared with other near-infrared surveys of molecular clouds. The regions that have been most extensively studied on a global scale are the Orion A and Orion B molecular clouds, and in both of these clouds, dense stellar clusters contribute significantly to the total young stellar population. In Orion B, approximately 96% of the stellar

population is found in just 4 clusters (Lada et al. 1991; Li, Evans, & Lada 1997). Similarly, in Orion A, at least 60% of the total stellar population is found within the Orion Nebula Cluster alone (Allen & Hillenbrand 2000; Meyer & Lada 2000), while the rest is distributed more uniformly throughout the molecular cloud and in several small clusters (Strom, Strom, & Merrill 1993). Near-infrared surveys of other molecular clouds are not as extensive as those in Orion and are biased toward known star forming regions, but nevertheless, observations of NGC 2264 (Lada, Young, & Greene 1993; Piche 1993) and NGC 1333 (Lada, Alves, & Lada 1996) also suggest that at least half of the stars within these regions form within clusters as opposed a more uniformly distributed population (see also the review by Clarke, Bonnell, & Hillenbrand 2000). While our survey is also not sensitive to any pervasive distributed stellar population, our results for the W3/W4/W5 region are similar to Orion in that a significant fraction of the cluster population is confined to just a few rich clusters.

4.2. Global Star Formation Characteristics

Of the 32 IRAS sources in our sample that were mosaicked at K' band, 21 are located in projection against the W3/W4/W5 H II region/molecular cloud complex (see Figure 2). The remaining 11 sources, or 34% of the sample, are separated from the W3/W4/W5 complex by as much as 100 pc. The molecular clouds associated with these 11 sources have radii of ≈ 0.5 pc with masses ranging from 27 $M_\odot$ to 410 $M_\odot$, with an average mass of 130 $M_\odot$. This contrasts with the massive star forming sites found in W3 that have cloud masses upwards of a few thousand solar masses or more.

Despite their relatively small mass, the 11 isolated clouds are not devoid of star formation nor is their stellar population limited to low mass stars. Eight of the 11 sources are forming a stellar cluster (see Table 2), and 3 sources (IRAS 01546+6319, 02044+6031, and 02561+6147) are associated with an early B type as indicated by the radio continuum emission. The fraction of the total cluster population found within these 11 clouds is 629/1595 = 39% despite the fact they have only $\approx 11\%$ of the total molecular mass as derived from the ^{13}CO observations. These percentages are likely upper limits since it is more difficult to identify IRAS point sources (and consequently clusters) near W3 than in more isolated regions. Indeed, the W3 Main cluster, two clusters a few arcminutes from W3(OH), and a cluster around BD +61 411 (Tieftrunk et al. 1998; Megeath et al. 1996) are found along the W3 ridge but were not identified with the IRAS point source selection criteria adopted in this paper. From visual inspection of the K band image presented in Tieftrunk et al. (1998), we estimate that these clusters in total may contain a few hundred stars. Even after accounting for these stars, the isolated clouds contribute a non-negligible fraction to the total cluster population currently forming in the W3/W4/W5 region.

The presence of massive stars and stellar clusters in these low mass clouds is somewhat surprising in that such characteristics are generally associated with massive GMCs. An interesting question is then how these isolated, star forming clouds originated. While the observations pre-

sented here cannot answer this question directly, we can speculate on their origin based upon the distribution of clouds in the vicinity of the W3/W4/W5 H II regions. The correspondence between the ^{12}CO and radio continuum emission shows that the H II regions have re-shaped the spatial distribution of molecular gas in some instances (see Figure 2). For example, the molecular gas near $(\ell, b) \approx (135^\circ, 0^\circ)$ wraps around the southern edge of the W4 H II region, and the cometary globule near $(\ell, b) \approx (134.8^\circ, 1.3^\circ)$ possibly formed from the interaction between the molecular gas and radiation pressure from OB stars in the W4 H II region (Heyer et al. 1996). The apparent effect of these interactions is that the small, dense globules of gas (which were either pre-existing or were formed by radiation pressure) remain for longer time scales than the more diffuse molecular material which is ionized or dispersed. Such globules are prominent in other OB associations and evolved H II regions as well, such as Orion OB 1 (Ogura & Sugitani 1998) and IC 1396 (Patel et al. 1998). It is tempting to speculate then that the isolated clouds tens of parsecs away from W3/W4/W5 are the last remnants of a GMC that has been dispersed by OB stars. In fact, the Per OB1 association occupies the area south of the W3/W4/W5 between $\ell = 130^\circ$ to $138^\circ$and $b = -5^\circ$ to -1° where several of the low mass clouds are found and is at nearly the same distance as the W3/W4/W5 H II regions (Garmany & Stencel 1992).

4.3. Massive Star Formation in W3

The W3 region has long been proposed as a classic example of induced or "triggered" star formation in molecular clouds. In this scenario, shocks arising from ionization fronts compress the ambient molecular material such that a gravitational instability develops in the post-shocked gas, leading to gravitational collapse and the formation of a new generation of stars. In the specific case of the W3 molecular cloud, it has been suggested that the expansion of the W4 H II region triggered the formation of W3 Main, W3(OH), W3 N, and AFGL 333, (Lada et al. 1978; Thronson, Campbell, & Hoffman 1980). Alternatively, it has been proposed that diffuse H II regions appear adjacent to embedded star forming sites because the associated dense molecular material has effectively slowed the expansion of the H II regions, and thus no cause and effect relationship exists between the H II regions and the newly formed stars. These two possibilities can be investigated with the data obtained for this study. If triggering is an important manner in which massive stars form, then embedded star forming regions throughout the W3/W4/W5 region should preferentially be located along the interfaces between ionization fronts and molecular clouds. Alternatively, if the expanding H II regions have had minimal impact on the massive star formation activity, then massive star forming regions should be located randomly throughout the W3 molecular cloud. Thronson, Campbell, & Hoffman (1980) cited similar arguments in suggesting that massive star formation has indeed been triggered in the W3 region, and we re-investigate this issue here using the more extensive and sensitive observations provided by IRAS and recent radio continuum surveys.

Of the molecular clouds in the W3/W4/W5 region, only the W3 molecular cloud extends tens of parsecs beyond the H II regions to provide a clear distinction between IRAS sources located near

and distant from the ionization fronts as seen in Figures 1 and 2. (Most of the IRAS sources in the W5 molecular cloud are located along the W5 H II region, consistent with the triggered star formation hypothesis. However, unlike the W3 region, the small extent of the W5 molecular cloud does not provide a "control" field unaffected by the ionization front.) The W3 molecular cloud extends for $\approx 60\,\mathrm{pc}$ and contains $\gtrsim 10^5\,\mathrm{M}_\odot$ of molecular material (Deane et al. 2000; Lada et al. 1978). Of the IRAS sources in our sample, the three most luminous sources are found along the interface between the W4 H II region and the W3 molecular cloud. This interface also includes the W3 Main (IRAS 02219+6152) massive star forming region (Megeath et al. 1996), which is not in our sample since this object is confused at $60\,\mu$m in the IRAS survey. By contrast, in the interior of the W3 cloud (i.e. west of the W4 ionization front), no IRAS sources are found that meet our selection criteria and have a far-infrared luminosity in excess of $500\,\mathrm{L}_\odot$.

Since W3 Main was not picked out by our IRAS selection criteria, we examine the possibility that massive star forming regions elsewhere in the W3 molecular cloud may also have been missed. Using the IRAS point source catalog, all sources were examined that have far-infrared luminosities in excess of $200\,\mathrm{L}_\odot$ but have low quality flux densities at $25\,\mu$m and/or $60\,\mu$m. Where appropriate, the reported upper limits were used in estimating the luminosity. All sources more luminous than $200\,\mathrm{L}_\odot$ were considered since two of the IRAS point sources in our sample are associated with a B type star despite having a low far-infrared luminosity (see Section 3.3). Using this search criteria, 12 additional sources were picked out in the W3 region. Eight of these sources are near W3 Main, W3(OH), or AFGL 333 and are confused at $60\,\mu$m and $100\,\mu$m, and one source is found midway between AFGL 333 and W3(OH). The other 4 IRAS sources are found interior to the cloud and are at least $30'$ (20 parsecs) from the W4 ionization front. Each of these four sources have far-infrared luminosities less than $430\,\mathrm{L}_\odot$, and none are associated with a NVSS radio continuum point source (Condon et al. 1998).

Recently, Ballantyne, Kerton, & Martin (2000) identified a massive O8 star that is ionizing an extended H II region near the southwestern edge of the W3 molecular cloud at (ℓ, b) $\approx (133.425^\circ, 0.055^\circ)$. The source is associated with extended far-infrared emission and is not listed as an IRAS 60μm point source, and possibly may represent a more evolved star forming region than the point sources analyzed here. This source is distant from the W4 ionization front and may indeed be an example of a massive star formation region that has formed spontaneously (Ballantyne, Kerton, & Martin 2000). Nonetheless, for the W3 molecular cloud as a whole, we conclude that the massive star forming regions are located preferentially (but not exclusively) along the W4 ionization front and are not randomly distributed throughout the cloud. This is quite remarkable considering that $\approx 75\%$ of the molecular mass in the W3 molecular cloud (based on the observed ^{12}CO(1–0) integrated intensity) is contained within the extended molecular gas component. These observations are thus consistent with the conjecture that massive star formation along the eastern edge of the W3 molecular cloud has been triggered by the W4 ionization front as previously proposed by Lada et al. (1978) and Thronson, Campbell, & Hoffman (1980).

5. Summary

We have analyzed the star formation properties of molecular clouds in the vicinity of the W3/W4/W5 H II regions using the FCRAO Outer Galaxy ^{12}CO(1–0) Survey, the IRAS point source catalog, published radio continuum observations, K' band imaging, and ^{13}CO(1–0) observations. We use these data to identify 34 IRAS point sources in the Perseus spiral arm that have far-infrared colors characteristic of embedded star forming regions. The stellar population associated with 32 of these IRAS sources are investigated based upon far-infrared and radio continuum emission and the identification of stellar clusters in the K' band mosaics. Our main conclusions are:

1. Nineteen stellar clusters are identified that contain a total of 1595 stars with K' magnitudes between $11.5^{\rm m}$ and $17.5^{\rm m}$. Approximately half of the total cluster population is found within the 5 richest clusters. Further, IRAS sources associated with embedded OB stars as traced by radio continuum emission contain 61% of the cluster population. Thus clusters around OB stars contribute substantially to the stellar population currently forming in the W3/W4/W5 region.

2. Eleven of the 32 IRAS point sources are located as far as 100 pc from the W3/W4/W5 H II region/molecular cloud complex. Despite the low average cloud mass ($130\,M_\odot$) associated with these 11 sources, three of these objects are associated with an OB star and 8 are forming a stellar cluster. These 11 clouds contain $\approx 39\%$ of the total stellar population identified in the IRAS sources, and thus contribute significantly to the current star formation production. We speculate that these clouds are the remnant fragments of a once large molecular cloud that has since been dispersed.

3. The conjecture that the W4 H II region as triggered star formation along the eastern edge of the W3 molecular cloud is re-investigated by analyzing the spatial distribution of star forming regions. We find that 4 of the 5 massive star forming sites in the W3 GMC, as traced by luminous IRAS point sources and/or radio continuum emission, are found along the interface between the W4 H II region and the W3 molecular cloud. The western portion of the W3 cloud, despite having $\approx 75\%$ of the molecular mass, contains only one known OB star forming region (Ballantyne, Kerton, & Martin 2000). These characteristics are consistent with the long-held notion that most of the massive star formation activity in the W3 molecular cloud has been induced by the expansion of the W4 H II region (Lada et al. 1978; Thronson, Campbell, & Hoffman 1980).

JMC acknowledges support from the James Clerk Maxwell Telescope Fellowship while part of this work was carried out, and current support from the Owens Valley Radio Observatory and Long Term Space Astrophysics Grant NAG5-8217. The Five College Radio Astronomy Observatory is operated with support from NSF grant 94–20159. This publication makes use of data products

from the Two Micron All Sky Survey, which is a joint project of the University of Massachusetts and the Infrared Processing and Analysis Center, funded by the National Aeronautics and Space Administration and the National Science Foundation.

REFERENCES

Allen, L. E., & Hillenbrand, L. A. 2000, to appear in "Proceedings of the Ringberg Castle Conference on Orion", PASP Conference proceedings, ed. M. McCaughrean, in press

Bachiller, R. & Cernicharo, J. 1986, A&A, 166, 283

Ballantyne, D. R., Kerton, C. R., & Martin, P. G. 2000, ApJ, accepted

Beichman, C. A., Myers, P. C., Emerson, J. P., Harris, S., Mathieu, P., Benson, P. J., & Jennings, R. E. 1986, ApJ, 307, 337

Carpenter, J. M., Meyer, M. R., Dougados, C., Strom, S. E., & Hillenbrand, L. A. 1997, AJ, 114, 198

Carpenter, J. M., Snell, R. L., & Schloerb, F. P. 1991, ApJ, 362, 147

Carpenter, J. M., Snell, R. L., Schloerb, F. P., & Skrutskie, M.F. 1993, ApJ, 407, 657

———. 1995, ApJ, 450, 201

Casali, M., & Hawarden, T. 1992, The UKIRT/JCMT Newsletter, No. 4, 33

Clarke, C. J., Bonnell, I. A., & Hillenbrand, L. A. 2000, in Protostars and Planets IV, ed. V. Mannings, A. P. Boss, and S. S. Russell (Tucson: University of Arizona Press), in press

Clemens, D. P., Sanders, D. B., & Scoville, N. Z. 1988, ApJ, 327, 139

Condon, J. J., Cotton, W. D., Greisen, E. W., Yin, Q. F., Perley, R. A., Taylor, G. B., & Broderick, J. J. 1998, AJ, 115, 1693

Dame et al. 1987, ApJ, 322, 706

Deane, J., Sanders, D. B., Carpenter, J. M., & Ladd, N. 2000, ApJ, in preparation

Deharveng, L., Zavagnoa, A., Cruz-Gonzalez, I., Salas, I., Caplan, J., & Carrasco, L. 1997, A&A, 317, 459

Digel, S. W., Lyder, D. A., Philbrick, A. J., Puche, D., & Thaddeus, P. 1996, ApJ, 458, 561

Elmegreen, B. G. 1992, in Star Formation in Stellar Systems, eds. G. Tenorio–Tagle, M. Prieto, & F. Sanchez, (Cambridge University Press:Cambridge), 381

Garmany, C. D., & Stencel, R. E. 1992, A&AS, 94, 211

Georgelin, Y. M., & Georgelin, Y. P. 1976, A&A, 49, 57

Heyer, M. H. et al. 1996, ApJ, 464, L175

Heyer, M. H., Snell, R. L., Brunt, C., Howe, J., Schloerb, F. P., & Carpenter, J. M. 1998, ApJS, 115, 241

Heyer, M. H.. & Terebey, S. 1998, ApJ, 502, 265

Hillenbrand, L. A., & Carpenter, J. M. 2000, ApJ, submitted

Hodapp, K. W. 1994, ApJS, 94, 615

Kenyon, S. J., Hartmann, L. W., Strom, K. M., & Strom, S. E. 1990, AJ, 99, 869

Kurtz, S., Churchwell, E., & Wood, D. O. S. 1994, ApJS, 91, 659

Lada, C. J., Alves, J., & Lada, E. A. 1996, AJ, 111, 1964

Lada, C. J., Elmegreen, B. G., Cong, H., & Thaddeus, P. 1978, ApJ, 226, L39

Lada, C. J., Young, E. T., & Greene, T. P. 1993, ApJ, 408, 471

Lada, E. A., DePoy, D. L., Evans, N. J. II, & Gatley, I. 1991, ApJ, 371, 171

Lee, Y., Snell, R. L., & Dickman, R. L. 1990, ApJ, 355, 536

Li, W., Evans, N. J. II, & Lada, E. A. 1997, ApJ, 488, 277

Massey, P., Johnson, K. E., & DeGioia-Eastwook, K. 1997, ApJ, 454, 151

Megeath, S. T., Herter, T., Beichman, C., Gautier, N., Hester, J. J., Rayner, J., & Shupe, D. 1996, A&A, 307, 775

Meyer, M. R., & Lada, E. A. to appear in "Proceedings of the Ringberg Castle Conference on Orion", PASP Conference proceedings, ed. M. McCaughrean, in press

McCutcheon, W. H., Sato, T., Dewdney, P. E., & Purton, C. R. 1991, AJ, 101, 1435

Miller, G. E., & Scalo, J. M. 1979, ApJS, 41, 513

Normandeau, M., Taylor, A. R., & Dewdney, P. E. 1996, Nature, 380, 687

_____. 1997, ApJS, 108, 279

Ogura, K., & Sugitani, K. 1998, Publ. Astron. Soc. Aust., 15, 91

Palla, F., & Stahler, S. W. 1993, ApJ, 418, 414

Panagia, N. 1973, AJ, 78, 929

Patel, N. A., Goldsmith, P. F., Heyer, M. H., Snell, R. L., & Pratap, P. 1998, ApJ, 507, 241

Piche, F. PASP, 105, 324

Strom, K. M., Strom, S. E., & Merrill, K. M. 1993, ApJ, 412, 233

Thronson, H. A. Jr., Campbell, M. F., & Hoffman, W. F. 1980, ApJ, 239, 533

Tieftrunk, A. R., Megeath, S. T., Wilson, T. L., & Rayner, J. T. 1998, A&A, 336, 991

Wainscoat, R. J., & Cowie, L. L. AJ, 103, 332

Weinberger, R. 1980, A&AS, 40, 123

Wouterloot, J. G. A., Brand, J., Burton, W. B., & Kwee, K. K. 1990, A&A, 230, 21

Vacca, W. D., Garmany, C. D., & Shull, J. M. 1996, ApJ, 460, 914

Fig. 1.— The location of the 34 IRAS point sources meeting our selection criteria (see text) overlaid on a grey scale image of the ^{12}CO(1-0) integrated intensity ($\int T_{\rm A}^{*} dv$) between $-57\,{\rm km\,s^{-1}}$ and $-32\,{\rm km\,s^{-1}}$ from the FCRAO Outer Galaxy Survey (Heyer et al. 1998). Small circles represent IRAS point sources with far-infrared luminosities $L_{\rm FIR} < 500\,L_{\odot}$, medium sized represent circles sources with $500\,L_{\odot} \leq L_{\rm FIR} < 5000\,L_{\odot}$, and large circles represent sources with $L_{\rm FIR} \geq 5000\,L_{\odot}$. The dash rectangle indicates the area that was searched for IRAS point sources. (For the astro-ph submission, Figure 1 is submitted as a JPEG image. See also http://astro.caltech.edu/∼jmc/papers/w3)

Fig. 2.— Contour map of the ^{12}CO(1-0) integrated intensity shown in Figure 1 overlaid on the $\lambda\,21\,\mathrm{cm}$ continuum image from the DRAO Galactic Plane Survey (Normandeau, Taylor, & Dewdney 1997). The contour level shown is for an integrated intensity of $\int T_{\mathrm{A}}^{*} dv = 12\,\mathrm{K\,km\,s^{-1}}$. (For the astro-ph submission, Figure 2 is submitted as a JPEG image. See also http://astro.caltech.edu/∼jmc/papers/w3)

Fig. 3.— Molecular line, near-infrared, and star count images for the 32 IRAS sources mosaicked at K' band. For each source, the left panel is an image of the ^{12}CO(1-0) integrated intensity ($\int T_{\rm A}^{*} dv$) from the FCRAO Outer Galaxy survey (Heyer et al. 1988) integrated over a $\pm$ 5 km s^{-1} interval around the velocity toward the IRAS source. Each ^{12}CO image is shown over a 30′× 30′ area centered on the IRAS point source position with a logarithmic intensity scale from $\log_{10}(1.0\,{\rm K\,km\,s^{-1}})$ to $\log_{10}(60.0\,{\rm K\,km\,s^{-1}})$. The adjacent panels show an image of the ^{13}CO(1-0) integrated intensity centered on the IRAS source, the K' band mosaic, and a K' band stellar surface density map for stars with magnitudes between 11.5$^{\rm m}$ and 17.5$^{\rm m}$. The contour levels for the ^{13}CO maps begin at $1.0\,{\rm K\,km\,s^{-1}}$ ($\int {\rm T_{MB}} dv$) with intervals of $2.0\,{\rm K\,km\,s^{-1}}$, except for IRAS 02232+6138, 02245+6115, 02310+6133, 02455+6034, 02459+6029, 02531+6032, 02570+6028, 02593+6016, and 02575+6017, which have intervals of $8.0\,{\rm K\,km\,s^{-1}}$. No ^{13}CO data are present in any of the maps for $\Delta\delta \geq 1.5'$. The contours in the stellar surface density images begin at 2σ above the mean derived stellar surface density (see text), with contours intervals of 3σ. (For the astro-ph submission, Figure 3 is submitted as JPEG images. See also http://astro.caltech.edu/∼jmc/papers/w3)

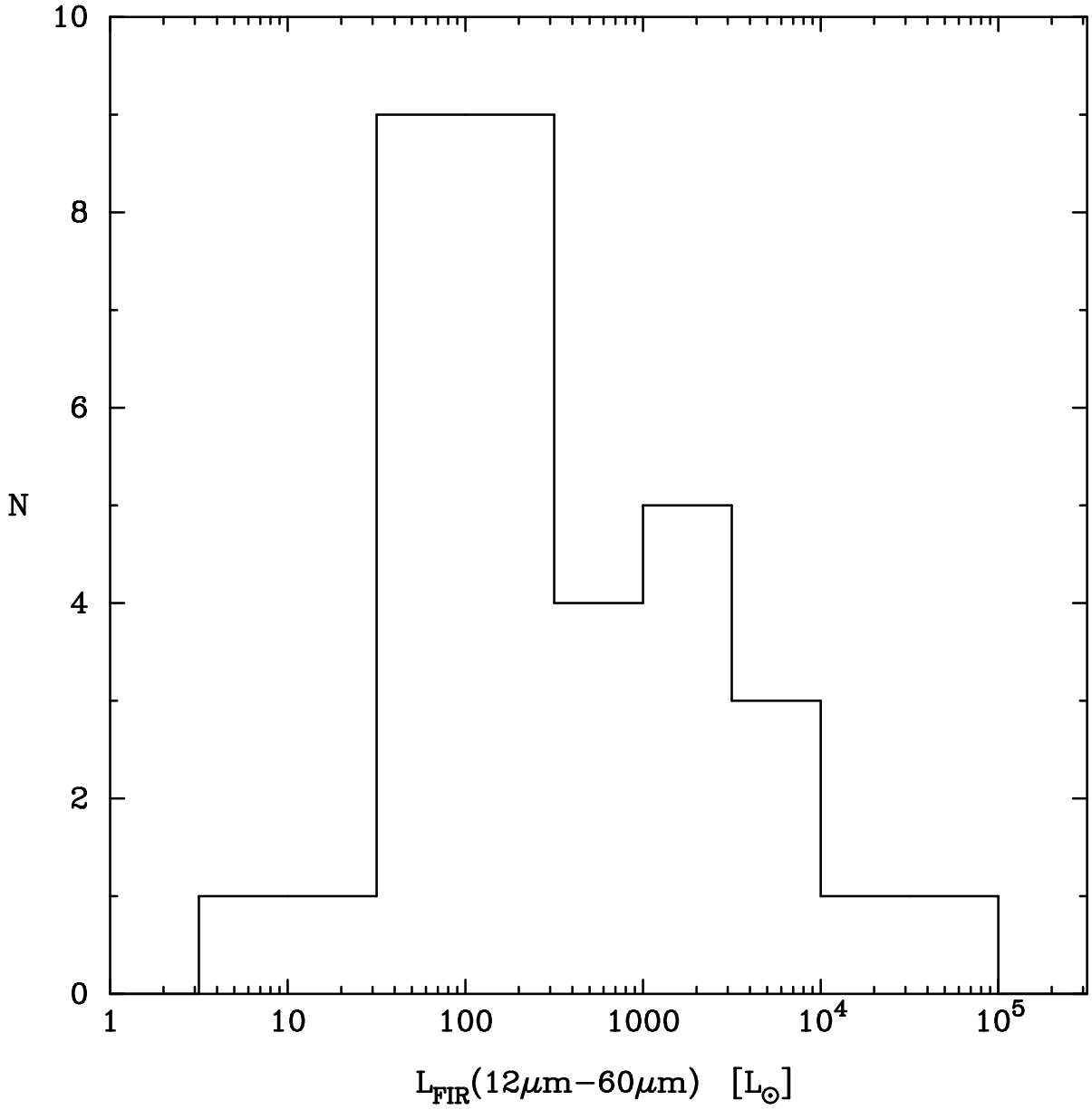

Fig. 4.— Histogram of the far-infrared luminosity in the 12 μm, 25 μm, and 60 μm IRAS bands for the 34 IRAS sources in our sample.

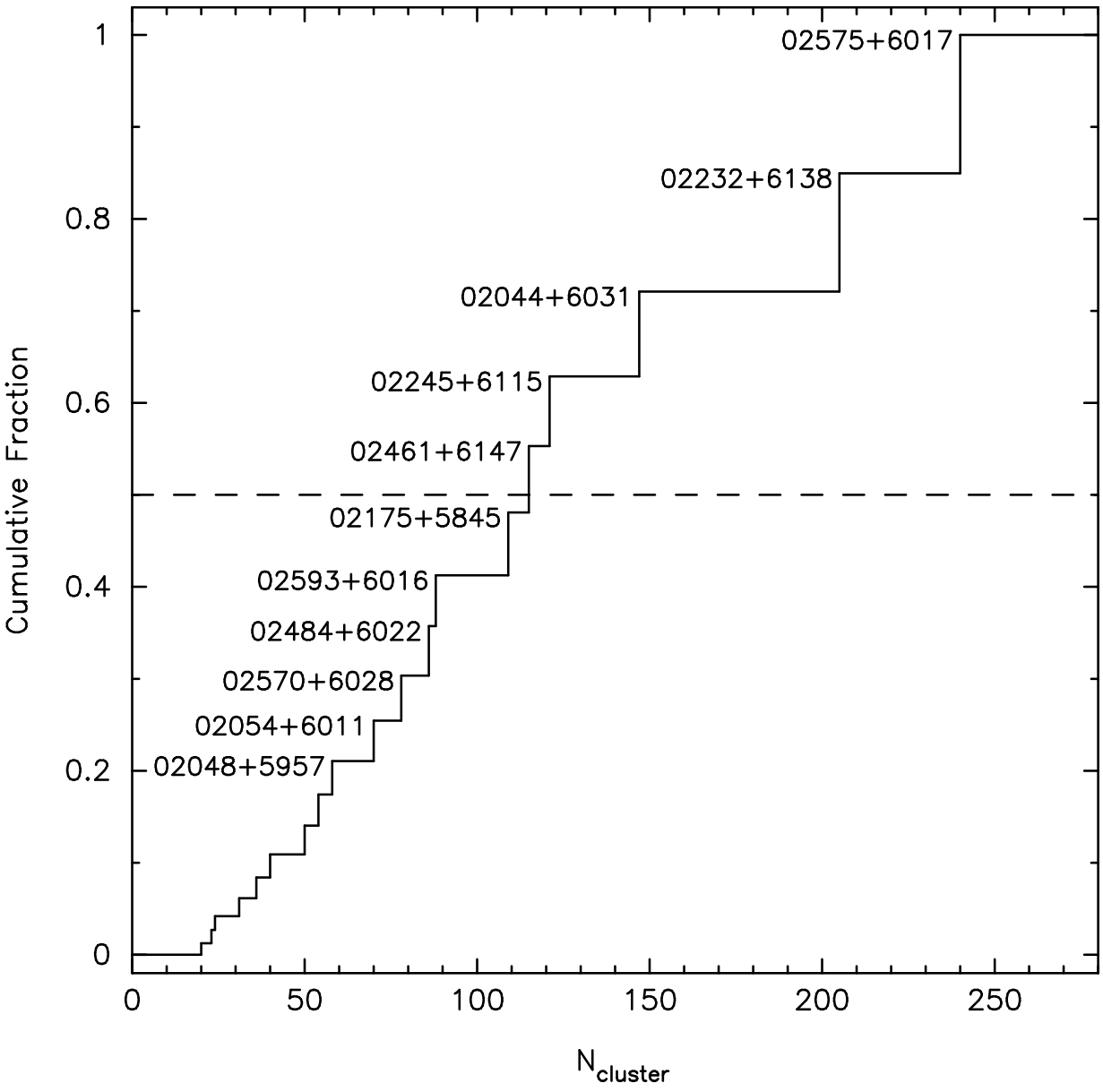

Fig. 5.— The cumulative distribution of the total number of stars identified in clusters as a function of the number of stars in an individual cluster. The star counts have been normalized by the total cluster population (1595 stars). The richest clusters are labeled by their IRAS point source name, and the horizontal dashed line shows the 50% point in the cluster population. These results indicate that half of the detected cluster population is found in just the five richest clusters.

Table 1. IRAS Sources in the W3/W4/W5 Region

IRAS	Galactic		Equatorial (J2000)		$V_{\rm LSR}$	Identification
	ℓ	b	α	δ	[km s^{-1}]	
01546+6319[a]	130.2939	1.6549	01:58:19.5	+63:33:59.1	-54	Weinberger 17
02008+6324[a]	130.9428	1.9137	02:04:34.3	+63:38:31.5	-45	
02044+6031[a]	132.1562	-0.7246	02:08:04.7	+60:46:01.5	-56	AFGL 5066
02048+5957[a]	132.3671	-1.2572	02:08:27.0	+60:11:45.6	-33	
02054+6011[a]	132.3684	-1.0212	02:09:01.3	+60:25:16.3	-57	
02081+6225[b]	132.0137	1.2156	02:11:49.7	+62:39:39.9	-54	
02175+5845	134.2729	-1.8974	02:21:07.7	+58:59:06.3	-48	Weinberger 18
02186+6053[a]	133.6888	0.1617	02:22:22.2	+61:07:11.3	-50	
02204+6128[b]	133.6961	0.7910	02:24:15.2	+61:42:26.6	-44	
02220+6107[a]	134.3365	0.8897	02:29:35.0	+61:34:07.8	-51	
02230+6202[a]	134.1165	1.7897	02:30:41.7	+62:29:10.0	-43	G133.8+1.4; W3 N
02232+6138[a]	133.9434	1.0595	02:27:01.0	+61:52:13.5	-46	W3(OH)
02245+6115[a]	134.2353	0.7485	02:28:21.5	+61:28:29.0	-49	AFGL 333
02310+6133[a]	134.8298	1.3120	02:34:46.8	+61:46:22.1	-40	
02327+6019[a]	135.5109	0.2576	02:36:33.5	+60:32:10.2	-43	
02379+5724[a]	137.2764	-2.1438	02:41:36.2	+57:37:37.0	-34	
02407+6047[a]	136.2220	1.0813	02:44:37.7	+60:59:52.7	-44	
02434+6018[a]	136.7205	0.7793	02:47:15.9	+60:30:44.2	-43	
02439+6025[a]	136.7309	0.9202	02:47:50.2	+60:38:05.5	-37	
02445+6042[a]	136.6723	1.2056	02:48:25.2	+60:55:02.9	-35	
02455+6034	136.8367	1.1367	02:49:23.2	+60:47:01.0	-40	
02455+5808	137.8969	-1.0490	02:49:21.1	+58:21:16.0	-46	
02459+6029	136.9172	1.0850	02:49:47.6	+60:42:06.9	-40	
02461+6147	136.3845	2.2690	02:50:09.2	+61:59:57.9	-44	AFGL 5085
02484+6022	137.2467	1.1153	02:52:18.7	+60:34:58.5	-57	
02495+6043	137.2148	1.4911	02:53:27.8	+60:55:58.1	-37	
02497+6217	136.5388	2.8947	02:53:44.4	+62:29:24.4	-48	
02511+6023	137.5407	1.2788	02:55:03.0	+60:35:44.3	-38	
02531+6032[a]	137.6937	1.5203	02:57:04.0	+60:44:22.3	-40	
02541+6208[a]	137.0682	3.0016	02:58:13.2	+62:20:29.0	-51	
02570+6028[a]	138.1514	1.6881	03:01:00.7	+60:40:20.3	-39	
02572+6006[a]	138.3477	1.3738	03:01:11.7	+60:18:08.7	-38	
02575+6017[a]	138.2913	1.5528	03:01:29.2	+60:29:11.8	-39	AFGL 4029
02593+6016[a]	138.4977	1.6409	03:03:17.9	+60:27:52.2	-39	Sh 201

[a]Coordinates of K' mosaic registered using the 2MASS Image Atlas

[b]Source not imaged at K' band

Table 2. Clusters Properties

IRAS	L_{FIR} ($L_\odot$)	SpT	Ref.[e]	R_{eff} (pc)	N_{stars}	$N_{cluster}$
01546+6319	260	B1	1	0.54	89	54 ± 6
02008+6324	9	···	···	···	···	
02044+6031	2900	B0	1	0.73	204	147 ± 8
02048+5957	120	···	···	0.56	94	58 ± 6
02054+6011	91	···	···	0.59	104	70 ± 6
02175+5845	220	···	···	0.73	168	109 ± 8
02186+6053	120	···	···	···	···	···
02220+6107	98	···	···	···	···	···
02230+6202	16000	O7	1	···	···	···
02232+6138[a]	46000	B0.5	1	0.91	281	205 ± 9
02245+6115	3300	B0.5	1	0.64	151	121 ± 6
02310+6133	270	···	···	···	···	···
02327+6019	270	···	···	0.32	30	20 ± 3
02379+5724	50	···	···	···	···	···
02407+6047	140	···	···	0.46	72	50 ± 5
02434+6018	770	···	···	0.37	39	24 ± 4
02439+6025	52	···	···	···	···	···
02445+6042	420	···	···	0.45	41	23 ± 4
02455+6034	1100	···	···	···	···	···
02455+5808	36	···	···	···	···	···
02459+6029	2000	···	···	0.45	48	31 ± 4
02461+6147	2300	B2	3	0.72	178	115 ± 8
02484+6022	88	···	···	0.62	140	86 ± 7
02495+6043	77	···	···	···	···	···
02497+6217	140	···	···	0.38	50	36 ± 4
02511+6023	210	B0.5	1	···	···	···
02531+6032	1200	B0.5	1	···	···	···
02541+6208	360	···	···	0.45	62	40 ± 5
02570+6028	530	···	···	0.62	114	78 ± 6
02572+6006	72	···	···	···	···	···
02575+6017[bcd]	5700	B1	2,4	1.00	340	240 ±10
02593+6016[d]	5800	O9.5	1	0.62	127	88 ± 6

[a]Observed at K band by Tieftrunk et al. (1998)

[b]Observed at K band by Deharveng et al. (1997)

[c]Observed at K band by Hodapp (1994)

[d]Observed at K band by Carpenter et al. (1993)

[e]References: (1) Condon et al. 1998; (2) Kurtz, Churchwell, & Wood 1994 (3) McCutcheon et al. 1991 (4) Carpenter, Snell, & Schloerb 1991

Table 3. Molecular Cloud Properties

IRAS	Radius (pc)	Mass ($M_\odot$)
01546+6319	0.49	27
02008+6324	0.60	64
02044+6031	0.49	140
02048+5957	0.32	29
02054+6011	0.51	100
02175+5845	0.68	410
02186+6053	> 0.89	> 600
02220+6107	0.37	69
02230+6202	> 1.06	> 670
02232+6138	> 0.99	> 2700
02245+6115	> 1.02	> 3200
02310+6133	> 0.77	> 680
02327+6019	0.69	410
02379+5724	0.51	71
02407+6047	0.70	290
02434+6018	0.42	120
02439+6025	0.28	29
02445+6042	> 1.03	> 920
02455+5808	> 0.47	> 45
02455+6034	> 0.69	> 670
02459+6029	> 0.80	> 800
02461+6147	0.34	83
02484+6022	0.63	43
02495+6043	0.47	69
02497+6217	0.49	55
02511+6023	0.45	130
02531+6032	> 0.47	> 290
02541+6208	0.42	56
02570+6028	0.53	380
02572+6006	0.40	28
02575+6017	0.69	870
02593+6016	> 0.51	> 300

This figure "figure1.jpg" is available in "jpg" format from:

http://arXiv.org/ps/astro-ph/0005237

This figure "figure2.jpg" is available in "jpg" format from:

http://arXiv.org/ps/astro-ph/0005237


This figure "figure3_a.jpg" is available in "jpg" format from:
http://arXiv.org/ps/astro-ph/0005237

This figure "figure3_b.jpg" is available in "jpg" format from:

http://arXiv.org/ps/astro-ph/0005237

This figure "figure3_c.jpg" is available in "jpg" format from:

http://arXiv.org/ps/astro-ph/0005237

This figure "figure3_d.jpg" is available in "jpg" format from:

http://arXiv.org/ps/astro-ph/0005237

This figure "figure3_e.jpg" is available in "jpg" format from:

http://arXiv.org/ps/astro-ph/0005237

This figure "figure3_f.jpg" is available in "jpg" format from:

http://arXiv.org/ps/astro-ph/0005237

This figure "figure3_g.jpg" is available in "jpg" format from:

http://arXiv.org/ps/astro-ph/0005237

This figure "figure3_h.jpg" is available in "jpg" format from:

http://arXiv.org/ps/astro-ph/0005237

This figure "figure3_i.jpg" is available in "jpg" format from:

http://arXiv.org/ps/astro-ph/0005237


This figure "figure3_j.jpg" is available in "jpg" format from:
http://arXiv.org/ps/astro-ph/0005237

This figure "figure3_k.jpg" is available in "jpg" format from:

http://arXiv.org/ps/astro-ph/0005237